Thermodynamic and kinetic stabilities of transmembrane helix bundles as revealed by single-pair FRET analysis: Effects of the number of membrane-spanning segments and cholesterol

Yoshiaki Yano, Yuta Watanabe, and Katsumi Matsuzaki*

Graduate School of Pharmaceutical Sciences, Kyoto University, Sakyo-ku, Kyoto 606-8501, Japan

AUTHOR INFORMATION

Corresponding Author

Katsumi Matsuzaki —*Graduate School of Pharmaceutical Sciences, Kyoto University, Sakyo-ku, Kyoto 606-8501, Japan*

Phone: +81-75-753-4521. Fax: +81-75-753-4578. E-mail: mkatsumi@pharm.kyoto-u.ac.jp

Authors

Yoshiaki Yano —*Graduate School of Pharmaceutical Sciences, Kyoto University, Sakyo-ku, Kyoto 606-8501, Japan*

Yuta Watanabe —*Graduate School of Pharmaceutical Sciences, Kyoto University, Sakyo-ku, Kyoto 606-8501, Japan*

Declaration of interest

The authors declare no financial competing interest.

Author contributions

Yoshiaki Yano: Conceptualization, Methodology, Writing-Original draft preparation, Funding acquisition **Yuta Watanabe**: Investigation, Writing-Original draft preparation **Katsumi Matsuzaki**: Conceptualization, Methodology, Writing-Review and Editing

ABSTRACT: The tertiary structures and conformational dynamics of transmembrane (TM) helical proteins are maintained by the interhelical interaction network in membranes, although it is complicated to analyze the underlying driving forces because the amino acid sequences can involve multiple and various types of interactions. To obtain insights into basal and common effects of the number of membrane-spanning segments and membrane cholesterol, we measured stabilities of helix bundles composed of simple TM helices $(AALALAA)_3$ (1TM) and $(AALALAA)_3$-G_5-$(AALALAA)_3$ (2TM). Association–dissociation dynamics for 1TM–1TM, 1TM–2TM, and 2TM–2TM pairs were monitored to compare stabilities of 2-, 3-, and 4-helical bundles, respectively, with single-pair fluorescence resonance energy transfer (sp-FRET) in liposome membranes. Both thermodynamic and kinetic stabilities of the helix bundles increased with a greater number of membrane-spanning segments in POPC. The presence of 30 mol% cholesterol strongly enhanced the formation of 1TM–1TM and 1TM–2TM bundles (~–9 kJ mol^{-1}), whereas it only weakly stabilized the 2TM–2TM bundle (~–3 kJ mol^{-1}). Fourier transform infrared-polarized attenuated total reflection (ATR-FTIR) spectroscopy revealed an ~30° tilt of the helix axis relative to bilayer

normal for the 1TM–2TM pair in the presence of cholesterol, suggesting the formation of a tilted helix bundle to release high lateral pressure at the center of cholesterol-containing membranes. These results demonstrate that the number of membrane-spanning segments affects the stability and structure of the helix bundle, and their cholesterol-dependences. Such information is useful to understand the basics of folding and assembly of multispanning TM proteins.

KEYWORDS: cholesterol, fluorescence resonance energy transfer, FTIR spectroscopy, helix bundle, number of membrane spanning, transmembrane helix

ABBREVIATIONS

1TM, $(AALALAA)_3$; 2TM, $(AALALAA)_3$-G_5-$(AALALAA)_3$; Biotin-PE, 1,2-dipalmitoyl-*sn*-glycero-3-phosphoethanolamine-*N*-(cap biotinyl); FTIR-PATR, Fourier transform infrared-polarized attenuated total reflection; LUVs, large unilamellar vesicles; PEG, poly (ethylene glycol); POPC, 1-palmitoyl-2-oleoyl-*sn*-glycero-3-phosphatidylcholine; sp-FRET, single-pair fluorescence resonance energy transfer; TM, transmembrane

Funding Sources

This work was supported in part by Grant-in-Aid for Scientific Research (C) (25460034 and 19K07013) from Japan Society for the Promotion of Science (JSPS).

1. INTRODUCTION

Multispanning transmembrane (TM) proteins play crucial roles in dynamic biological processes such as signal transduction, material transport, and energy conversion. For example, 7-TM receptors rapidly transduce information from external signals to the inside of cells, typically via coupling to G-proteins, in response to binding of their ligands to the receptors [1–4]. Conformational changes of proteins are essential for the function of membrane proteins, typically involving rearrangement of the TM helices in the helix bundle. For rapid responses to biological stimulations, it is important to balance thermodynamic stability of the inactive conformation before stimulation and kinetic instability of the conformation after stimulation.

In lipid bilayer environments, the thermodynamic and kinetic stabilities of TM helical bundles should be determined by a balance of helix–helix, helix–lipid, and lipid–lipid interactions. Both helix-involved and lipid-involved terms can include various types of interactions depending on the amino acid sequences and lipid compositions, respectively. Measurements of conformational dynamics of membrane proteins, particularly single molecule observations, have revealed a wide range of kinetic stabilities of individual conformations from microseconds to weeks, depending on the amino acid sequences [1, 4–10]. Membrane properties should also significantly affect these dynamic stabilities, because the lipid compositions of membranes are often critical for the functions of membrane proteins [11–14]. However, it is not easy to assess the relative importance of underlying driving forces that determine stabilities of the helix bundles in membranes.

The use of model transmembrane helices is a straightforward approach to separately examine sequence-independent (common, basal, general, or nonspecific) properties and sequence-dependent properties of TM helices. Self-association of synthetic peptides with naturally occurring and de-novo designed amino acid sequences have elucidated driving forces for the stabilization of TM proteins, originating from the amino acid sequences and lipid compositions [15–22].

An important aspect to understand the basics on the stability of TM helix bundles in lipid bilayers is the general effects of the number of membrane-spanning segments. When multiple TM helices are assembled into a bundle, the proportion of helix–helix contacts increases at the expense of helix–lipid contacts with the number of membrane-spanning segments in the bundle. Thermodynamic/dynamic measurements are important to clarify how this change generates size-dependent interactions, and how membrane lipids affect these interactions. Here, we examined these issues using the model TM helix $(AALALAA)_3$ (1TM), composed of only inert Ala and Leu side chains, as a simple helix unit. Previous studies showed that 1TM adopts stable transmembrane helical structures in various membrane lipid compositions [23–25]. Hydrophobic mismatch between PC membranes with different acyl chain lengths (hydrophobic thicknesses of 20–34 Å) and the helix (hydrophobic length of 27–29 Å) did not significantly affect the orientation of the helix [24]. The 1TM helices self-associate to preferentially form antiparallel dimers due to attraction between helix macrodipoles, the strength of which was enhanced in thicker membranes due to lower dielectric constants at the helix termini [24]. Small headgroup lipids such as phosphoethanolamine and cholesterol enhance the 1TM–1TM association by changing the physico-chemical properties of membranes [23, 25]. The helix side-chain interactions do not significantly contribute to stabilization of the 1TM dimer, although the sequence includes a number of Ala residues, small residues (Gly, Ala, Ser) that are often observed at helix–helix contacts in membrane proteins [26–28]. The presence of Gly residues can also induce deviation from a straight α-helix of TM helix of cytochrome-b5 and it may affect its interaction with TM helices of cytochrome-P450 [29, 30]. On the other hand, introduction of a GXXXG motif into 1TM significantly enhances dimerization of the helices [31]. These results demonstrate that the 1TM helix represents common and basal properties of TM helices with minimal sequence-dependent characters. Thermodynamic/dynamic data on the dimerization processes of 1TM are advantageous for discussing driving forces that stabilize TM helix bundles with different numbers of segments. Such

quantitative information provides fundamental data to understand stabilities of TM proteins. It is also useful as a benchmark of computer simulation studies to examine effects of membrane physico-chemical properties on the associations of TM helices in molecular detail [32–34]. Furthermore, the association of TM helices in membranes is also of interest to those studying antimicrobial peptides which form barrel-stave TM pores. We note that the limitations in using such results to generally understand the TM–TM interactions in real membrane proteins/peptides, because the use of $(AALALAA)_3$ helices only report rather basal properties of TM helices, and natural TM sequences can include more complex interactions.

To examine the stability of TM helix bundles by single-pair fluorescence resonance energy transfer (sp-FRET) measurements in lipid vesicles, we designed the $(AALALAA)_3$-G_5-$(AALALAA)_3$ (2TM) peptide, which is composed of two 1TM helices connected with a flexible pentaglycine linker (~18 Å in extended conformation). Introduction of the linker between the two helices was considered to restrict relative translational motion of the two helices in the bilayer, although it does not contribute to the formation of a specific loop structure. Association–dissociation processes for 1TM–1TM, 1TM–2TM, and 2TM–2TM pairs were monitored to evaluate stabilities of 2-, 3-, and 4-helix bundles, respectively. Significant helix macrodipole attractions are expected for 1TM–1TM and 2TM–2TM associations, whereas they should be net ineffective for the 1TM–2TM association, because an attractive force between 1TM and the first helix of 2TM is canceled out by a repulsive force between 1TM and the second helix of 2TM (vide infra). The obtained dynamic/thermodynamic data are used to evaluate various driving forces that stabilize these TM helix bundles.

2. EXPERIMENTAL PROCEDURES

Materials. Chromophore-labeled peptides X-(AALALAA)$_3$- NH_2 [X = NBD (**I**); X = Cy3B (**II**); X = Cy5 (**III**)] and X-(AALALAA)$_3$-G$_5$-(AALALAA)$_3$- NH_2 [X = NBD (**IV**); X = Cy3B (**V**); X = Cy5 (**VI**)] were synthesized by the standard 9-fluorenylmethoxycarbonyl-based method on a NovaSynTGR resin (Milipore, Billerca, MA, USA). The structures of fluorophores are shown in Supporting Figure S1. The fluorophores were labeled at the N-termini on the resin by treatment with succinimidyl ester derivatives of the fluorophores (2–3 equiv, purchased from GE Healthcare, Little Chalfont, UK) in *N*,*N*-dimethylformamide containing 5% *N*,*N*-diisopropylethylamine for 48 h. The peptides were purified by a PLRP-S 300 Å 5 μm reversed phase column (Agilent Technologies, Santa Clare, CA, USA) with a linear gradient from formic acid/H_2O (2/3, v/v) to formic acid/2-propanol (4/1, v/v) at 50°C. To prevent degradation of the fluorophores, the eluted peptide solution was immediately neutralized with 28% NH_3 (aq) on ice, followed by lyophilization. The peptide powder was dissolved in 1,1,1,3,3,3-hexafluoroisopropanol and identified by matrix-assisted ionization mass spectroscopy. The purity of the peptides was higher than 90% (Supporting Figure S2). Cholesterol, 1-palmitoyl-2-oleoyl-*sn*-glycero-3-phosphatidylcholine (POPC), and 1,2-dipalmitoyl-*sn*-glycero-3-phosphoethanolamine-N-(cap biotinyl) (biotin-PE) were obtained from Avanti (Alabaster, AL, USA). Neutravidin was a product of Thermo Scientific (Waltham, MA, USA). Poly(ethylene glycol) (PEG)-coating reagents were obtained from Laysan Bio (Arab, AL, USA). Spectrograde organic solvents were products of Nacalai Tesque (Kyoto, Japan). Other chemicals were obtained from Sigma-Aldrich (St. Louis, MO, USA) unless otherwise stated. Cholesterol and POPC were dissolved in ethanol and chloroform, respectively, and their concentrations were determined in triplicate by the cholesterol oxidase method [Free Cholesterol E-Test kit (Wako, Tokyo, Japan)] and phosphorus analysis, [35] respectively.

FTIR Spectroscopy. Oriented films of lipids and peptides were prepared by uniformly spreading a 50 μL ethanol solution of lipids (5 μmol) and peptides (5 nmol) on a germanium ATR plate (70 ×

10 × 5 mm), followed by evaporation of the solvent under a vacuum overnight. The films were hydrated with a D_2O-soaked piece of filter paper put over the plate for 4 h at 25℃. Fourier transform infrared-polarized attenuated total reflection (FTIR-PATR) measurements were conducted as described previously [23] on a Bruker TENSOR27 spectrometer equipped with a Specac Horizontal ATR attachment with an AgBr polarizer and a temperature controller. The dichroic ratio, R, defined by $\Delta A_{\parallel}/\Delta A_{\perp}$, was calculated from the polarized spectra. The absorbance (ΔA) was obtained as the area for the amide I band. Subscripts ∥ and ⊥ refer to polarized light with the electric vector parallel and perpendicular to the plane of incidence, respectively. The average helix orientation angle to the bilayer normal, α, was calculated from R:

$$\cos^2\alpha = \frac{1}{3}\left(\frac{4}{3\cos^2\theta - 1}\frac{R - 2.00}{R + 1.45} + 1\right) \qquad (1)$$

We assumed a fixed angle (θ) of 35° between the helix axis and transition moments for amide I bands [36].

Liposome Preparation. Large unilamellar vesicles (LUVs) were prepared by an extrusion method using a buffer containing 10 mM Tris, 150 mM NaCl, and 1 mM EDTA (pH 7.4) (TE buffer), as described in a previous report [23]. Hydration and extrusion were performed at ~50℃ to ensure the mixing of membrane components.

Sp-FRET. The biotin-PEG-coated slide chamber for fixing LUVs was prepared according to the protocol of Joo and Ha [37]. Briefly, No. 1-S cover glass (Matsunami Glass, Osaka, Japan) was washed with 1 M KOH and methanol, amino-functionalized by aminopropylsilane, and coated with biotinylated PEG by treatment with PEG-succinimidyl ester, with an average MW of 5000 (mPEG-

SVA), and its biotin derivative (biotin-PEG-SVA) at a ratio of 80/1 (w/w). The helices labeled with Cy3B and Cy5 at N-termini were incorporated into LUVs (total lipid concentration of 5 mM) at a **II** or **V**/**III** or **VI**/lipid/biotin-PE molar ratio of 1/1/90,000/900 (an approx. peptide/lipid ratio of 2/90,000). In this study, the three donor–acceptor peptide pairs **II**–**III**, **V**–**III**, and **V**–**VI** were examined to measure 1TM–1TM, 1TM–2TM, and 2TM–2TM interactions, respectively. The biotinylated LUVs were diluted to 10 μM lipids, added onto the biotin-PEG-coated glass surface, and incubated for 1 min after a 10-min pretreatment with 0.2 mg mL^{-1} NeutrAvidin. This procedure typically resulted in 200–400 vesicles in the analyzed area (80 × 80 μm). The fluorescence images for Cy3B (575–635 nm) and Cy5 (645–745 nm) under Cy3B excitation at 561 nm were simultaneously acquired using an ImagEM EM-CCD camera with W-View optics (Hamamatsu Photonics, Hamamatsu, Japan) under a Nikon (Tokyo, Japan) Ti-based total internal reflection fluorescence microscope with a time resolution of 17 ms. To suppress photoblinking, the observation was performed in TB buffer containing 1 mM trolox, 1 mM methyl viologen, 0.8 % (w/v) D-glucose, 0.25 mg mL^{-1} glucose oxidase, and 10.5 mg mL^{-1} catalase (pH 7.4). The apparent FRET efficiency, E_{app}, was calculated from fluorescence intensities for the donor (F_{Cy3B}) and acceptor (F_{Cy5}) as $E_{app} = F_{Cy5} / (F_{Cy3B} + F_{Cy5})$. The sp-FRET trajectories originating from the monomer–dimer transitions were analyzed with the HaMMy program [38] (http://bio.physics.illinois.edu/HaMMy.asp) to deduce the rate constants between different states. Assuming two state dynamics, the rate constants for dimer formation (k_{on}) and dimer dissociation (k_{off}) were obtained from k = (transition probabilities)*(data acquisition rate (Hz)). The fraction of associated helices (f_a) was estimated from the rate constants:

$$f_a = \frac{k_{on}}{k_{on} + k_{off}} \qquad (2)$$

The association constant (K_a) and corresponding Gibbs free-energy change (ΔG_a) are given by:

$$\Delta G_a = -RT \ln K_a \qquad (3)$$

$$K_a = \frac{[\mathrm{D}]}{[\mathrm{M}]^2} \qquad (4)$$

R and T represent the gas constant and absolute temperature, respectively. [M] and [D] denote the mole fraction of the helix monomer and dimer in the bilayers, respectively, which are related to f_a as:

$$[\mathrm{M}] = (1 - f_a)\frac{2n_p}{2n_p + n_l} \qquad (5)$$

$$[\mathrm{D}] = \frac{f_a n_p}{2n_p + n_l} \qquad (6)$$

the number of peptides (= 2) and lipids (= 90,000) in a vesicle are denoted by n_p and n_l, respectively. The factor of 2 is introduced to take the TM nature of the peptide into consideration.

The temperature dependence of the thermodynamic parameters for self-association was analyzed by:

$$\Delta G_a = \Delta H_a - T\Delta S_a \qquad (7)$$

3. RESULTS

Sp-FRET Measurements. The sp-FRET technique is suitable for monitoring the dynamics of biomolecules in timescales of milliseconds to seconds, although the use of fluorescent dye has some intrinsic limitations when accurately measuring the thermodynamic parameters for helical association and the effect of cholesterol. We successfully detected sp-FRET signals for association of pairs of TM helices confined in liposome membranes, where $\Delta G_a \leq$ ~–20 kJ mol^{-1} [23, 31]. The sp-FRET measurements were performed using Cy3B and Cy5 fluorophores as FRET donor and acceptor, respectively (donor: **II**, **V**, and acceptor: **III, VI**). The Cy3B–Cy5 pair can effectively detect peptide dimers due to its long R_0 of 67 Å, even if the fluorophores are separated across the membrane in an antiparallel dimer. For single-molecule detection, we used a very low peptide/lipid ratio such that one liposome included two peptides on average (peptide mole fraction ~4×10^{-5}). Biotin–avidin interaction was used to attach the liposomes on a glass surface (Figure 1a). The fluorescence time-lapse images for Cy3B and Cy5 channels were simultaneously obtained under excitation of Cy3B. An anticorrelation of the fluorescence intensities of the two channels indicates FRET fluctuation. Dimer formation and dissociation of the dimer were detected as a stepwise decrease in donor fluorescence intensity with a simultaneous increase in acceptor fluorescence intensity and a stepwise recovery of the donor emission and concomitant disappearance of the acceptor emission, respectively (Figure 1b). After the measurements, the number of helices was determined by stepwise photobleaching (Figures 1c and d). Kinetic analysis was performed for liposomes that had incorporated only one Cy3B and one Cy5 molecules.

In POPC vesicles, 1TM–1TM did not show any detectable FRET signals over the time-course (Figure 1b), being consistent with a previous study [23]. This is because the association–dissociation dynamics of 1TM were too rapid to detect the formation of its dimer within the resolution of sp-FRET (~17 ms), although 1TM helices weakly self-associate in POPC [25]. On the other hand, 1TM–2TM and 2TM–2TM pairs clearly exhibited FRET fluctuation trajectories with

durations of residencies of subseconds, reflecting dynamic monomer–dimer equilibria. In POPC/cholesterol (7/3) vesicles, in addition to the 1TM–2TM and 2TM–2TM pairs, the 1TM–1TM pair exhibited FRET signals, as reported in a previous study [23].

Kinetic parameters for formation of the dimer and its dissociation into monomers were analyzed by HaMMy fitting program [38]. An example of the fitting is shown in Figure 2a. The rate constants for dimer formation (k_{on}) and dissociation (k_{off}) (Figure 2b) were calculated from the obtained transition probabilities for the formation of 2TM–1TM and 2TM–2TM in POPC. The ln (k) distributions underwent Gaussian fitting to obtain the center values and half-widths, and they were defined as the average rate constants and measurement errors, respectively. The lifetimes of the monomers and dimers were obtained by calculating the inverse of the average rate constants (Table 1), and ΔG_a values (Table 2) were calculated by Eqs. (2)–(6). Both monomer and dimer lifetimes increased with the number of membrane-spanning segments (Table 1). The size-dependent difference in the lateral diffusion of the 1TM vs. 2TM helices may affect the association rate of the helices. However, this effect should be small because the diffusion coefficients of transmembrane proteins scale with ln (1/R), where R is the hydrodynamic radius, consistent with the Saffman-Delbrück model [39]. Even a doubling of R decreases k_{on} only by ~30% and thus increases the ΔG_a value by ~1 kJ mol^{-1}. Figure 2c shows histograms of the apparent FRET efficiency, E_{app}, that were obtained from the donor fluorescence intensity, F_{Cy3B}, and the acceptor fluorescence intensity, F_{Cy5}, for all vesicles containing a donor–acceptor pair. Note that the associated fraction f_a (Eq. (2)) can also be estimated from curve fitting of the histograms of E_{app} values (Figure 2c). We confirmed that similar f_a values were obtained from the rate constants and the curve fitting of E_{app} distribution (data not shown). The self-association of 1TM was not detected by sp-FRET measurements as stated above, although the previous ensemble FRET measurements estimated an association free energy of $\Delta G_a = -13.2 \pm 0.2$ kJ mol^{-1} at 298 K [25]. For 1TM–2TM and 2TM–2TM associations, ΔG_a values were -19.3 ± 1.2 and -21.6 ± 2.2 kJ mol^{-}

[1], respectively. The association was stronger as the number of membrane-spanning segments increased in the order of 1TM–1TM, 1TM–2TM, and 2TM–2TM.

Similar measurements were performed in POPC/cholesterol (7/3) vesicles (Figure 3). The results showed significant effects of cholesterol on the formation of TM helix bundles. Overall, the lifetimes of monomers and dimers decreased and increased, respectively, in the presence of cholesterol for 1TM–2TM and 2TM–2TM associations (Table 1). Introduction of 30 mol% membrane cholesterol typically decrease lateral diffusion of single TM proteins by ~30% [40–42]. This effect on ΔG_a is not significant (~1 kJ mol^{-1}). The dimer lifetime increased with the number of membrane-spanning segments, similar to the case in POPC, whereas the monomer lifetime was noticeably shorter for the 1TM–2TM association (Table 1). For the 1TM–1TM association, the ΔG_a value was –22.1 ± 1.9 kJ mol^{-1}, which is consistent with the one obtained from ensemble FRET measurements in a previous report (–22.6 ± 0.1 kJ mol^{-1}) [23]. For the formation of 1TM–2TM and 2TM–2TM bundles, the ΔG_a values were –28.3 ± 2.6 and –24.2 ± 3.1 kJ mol^{-1}, respectively. In contrast to the results in the absence of cholesterol, the association was stronger in the order of 1TM–1TM, 2TM–2TM, and 1TM–2TM, because cholesterol prominently stabilized the 1TM–1TM and 1TM–2TM bundles, whereas it was less effective for the formation of the 2TM–2TM bundle.

To analyze the association of enthalpy and entropy values, sp-FRET measurements were performed at 20, 25, 30, and 35°C (Figure 4). The thermodynamic parameters were estimated from linear regression according to Eq. (7). The thermodynamic parameters at 25°C are summarized in Table 2.

FTIR-PATR Measurements. FTIR-PATR spectroscopy was conducted to confirm the helical and transmembrane structures of the peptides in bilayers prepared on a Ge ATR plate. Bilayers composed of POPC only or POPC/cholesterol (7/3) were used to clarify the effects of cholesterol on the properties of transmembrane helices. To examine the differences of helix orientations

depending on the number of membrane-spanning segments, three peptide compositions were measured: only **I** (1TM), **I**–**IV** (1TM/2TM(1/1)), and only **IV** (2TM). The quantity of peptides required for the FTIR measurements (5 nmol/sample) was larger than that for the sp-FRET measurements (~0.1 nmol/sample). We used peptides labeled with NBD, instead of Cy3B- or Cy5, for quantification of the peptides by the absorbance. The attachment of the NBD group at the N-terminus did not affect the conformation or the orientation of the helix [36]. The dimer fraction f_a was much higher in the FTIR measurements compared with that in the sp-FRET measurements because the peptide concentration was two orders of magnitude higher (peptide mole fraction ~2×10^{-3}) than that in sp-FRET measurements (peptide mole fraction ~4×10^{-5}). The f_a value was estimated to be 0.35 for the weakest 1TM–1TM association in POPC (ΔG_a = –13.2 kJ mol^{-1}, Table 2), whereas it was in the range of 0.73–0.95 for the other conditions (ΔG_a = –19.3—28.3 kJ mol^{-1}, Table 2). Therefore, the measured spectra principally originate from the peptide dimers except in the case of 1TM in POPC. The hydrophobic length of the TM helix $(AALALAA)_3$ (27–29 Å) matches to the hydrophobic thickness of POPC bilayers (thickness, ~27 Å), although the thickness slightly increases in the presence of cholesterol (3–4 Å [43]) because of the acyl chain ordering.

Figure 5 shows the amide region spectra for 1TM, 1TM/2TM(1/1) or 2TM incorporated into membranes at 25°C. In both POPC and POPC/cholesterol(7/3) bilayers, amide I and II absorption bands were narrow (half width, ~18 cm^{-1}), suggesting a homogenous secondary structure. The peak wavenumbers around 1660 cm^{-1} indicate the formation of helices. Table 3 summarizes the dichroic ratios R ($\Delta A_{\parallel}/\Delta A_{\infty}$) ($n$ = 3). These R values were larger than the value for random orientation (R = 2), confirming that the helices had a tendency to assume transmembrane orientations. The decomposition of the amide I bands failed to resolve signals from the Gly loop, probably because their contributions were only 7.4 and 10.6% for 1TM/2TM and 2TM systems, respectively, and some turn structures exhibit absorption around 1660 cm^{-1} [44]. The amide I/amide II absorption ratios were similar in both lipid compositions, indicating that the helices were embedded in the

membrane and protected from significant H/D exchange. The average orientation angles α of the helix axis relative to the bilayer normal were calculated from the *R* values (Table 3). Of note, in the presence of cholesterol, 1TM and 1TM/2TM showed significantly larger helix tilts (17 ± 2° and 30 ± 1°, respectively) than those in pure POPC (~0° and 15 ± 3°, respectively), indicating significant conformational change of the 2- and 3-TM helix bundles induced by cholesterol. On the other hand, 2TM did not show a difference in orientation between these two membranes (~22°). This suggests that the structures of 2TM in POPC/cholesterol and pure POPC membranes are similar, although it does not necessarily guarantee that the interfaces of helix contacts are identical.

4. DISCUSSION

1TM–1TM bundle. In previous studies, we revealed that helix macrodipole attraction dominates the driving force for formation of the 1TM–1TM dimer in POPC bilayers [23, 25]. The strength of dipole–dipole interaction can be estimated from the following equation:

$$w = -\frac{\mu_1 \mu_2}{4\pi\varepsilon_0 \varepsilon r^3}(2\cos\theta_1\cos\theta_2 - \sin\theta_1\sin\theta_2\cos\phi) \qquad (9)$$

where μ,ε_0, ε, and r represent the helix dipole moment (= 2.5×10^{-28} Cm), dielectric constant in a vacuum, relative dielectric constant, and distance between dipoles (= 10 Å), respectively. The angles θ_1 and θ_2 are angles between a vector that connects the centers of two dipoles and axes of the first and second dipoles, respectively. Angle ϕ indicates a torsion angle between the dipoles. In the case of an antiparallel dimer in POPC with a helix orientation angle of ~0°, the parameters ϕ, θ_1 and θ_2 were fixed at 0°, 90°, and 270°, respectively. The value of ε at the helix termini was assumed to be 15 [25]. The calculated energy of –23 kJ mol^{-1} is identical to the observed ΔH_a value

(–23.7 ± 0.4 kJ mol^{-1}, Table 2), suggesting that the effects of side-chain packing and lipid-involved (helix–lipid and lipid–lipid) contacts are small for the 1TM–1TM association in POPC bilayers. The major contribution to the $-T\Delta S_a$ term originates from losses of the translational and rotational degrees of freedom upon helix association (up to +8 kJ mol^{-1}) [45]. The contribution of side-chain packing to $-T\Delta S_a$ was indirectly estimated to be a small positive value of ~+2 (= +10 – 8) kJ mol^{-1}. We also consider that energetic contributions from the lipid-involved interactions were ~0 in POPC in the following analyses for 1TM–2TM and 2TM–2TM associations.

In the presence of cholesterol, a number of driving forces significantly contribute to the association free energy ($\Delta\Delta G_a$ = –9 kJ mol^{-1}, Table 2), as previously discussed in detail [45], and are summarized as follows. A rigid sterol ring and small polar headgroup (-OH) of cholesterol markedly affect physico-chemical properties of the lipid bilayers in various manners. POPC/cholesterol (7/3) membranes have been proposed to submicroscopically demix into l_d/l_o states; however, they do not exhibit macroscopic phase separation [46]. Cholesterol also plays an important role on the membrane binding, topology and mechanism of membrane disruption by the antimicrobial peptide pardaxin [47]. Solid state NMR results have reported a role of cholesterol on the helical tilt of pardaxin [48]. Fluorescence quenching experiments using a fluorescent sterol analog have shown that 1TM helices and sterols are randomly distributed on the membrane plane (see Figure S2 of Ref. [31]). Therefore, we considered that the mixture was in a single phase. Membrane cholesterol orders fluid bilayers [49]. Incorporation of 30 mol% of cholesterol slightly increases the hydrophobic thickness of the lipid bilayers by the acyl chain ordering (~4 Å) compared with that of pure POPC (~27 Å) [43]. The thicker membrane can lower polarity at the termini of the incorporated TM helix to strengthen helix macrodipole interactions (~–2kJ mol^{-1}) [23]. The sterol also tends to preferentially interact with POPC compared with the $(AALALAA)_3$ helix because both cholesterol and the helix have rigid structures [23]. This can be an indirect driving force for helix association that involves a decrease in helix–cholesterol contacts and an

increase in POPC–cholesterol contacts [23]. Furthermore, membrane cholesterol imposes another membranous force that originates from the lateral pressure profile (or curvature strain) from the imbalance between cross sections of the headgroup and hydrocarbon core regions (Figure 6) [14, 50, 51]. Due to the small headgroup of cholesterol, the headgroup and hydrocarbon core regions have lower and higher lateral pressures, respectively, in cholesterol-containing membranes compared with pure POPC membranes. A higher lateral pressure in the hydrocarbon core due to cholesterol can be partially released by the formation of an hourglass-shaped dimer, consistent with the observed larger helix tilt (17 ± 2°, Table 3) [23].

1TM–2TM bundle. In contrast to the case of the 1TM–1TM bundle, helix macrodipole interactions do not effectively drive the formation of the 1TM–2TM bundle (Figure 7a). Therefore, the strength of macrodipole interaction was considered to be zero. Instead, the helix packing interaction should be a principal driving force for the formation of the 1TM–2TM bundle in POPC. We attributed the observed ΔH_a = –35 kJ mol^{-1} to the contribution of helix packing. Assuming motional contributions of +8 kJ mol^{-1} to $-T\Delta S_a$ term, the effect of helix packing on the entropic term was indirectly estimated to be +8 (= 16 – 8) kJ mol^{-1}. Barth and colleagues reported motif sequences that contribute to efficient helix packing for the TM helix trimer [52]. The helix $(AALALAA)_3$ involves a number of AXXXA motifs, which can stabilize TM 3-helix bundles. The observed helix orientation angle (15 ± 3°, Table 3) is consistent with those in the helix trimers involving the motifs (all-right type, 18 ± 5°, calculated as half values of the crossing angles) [52]. Our results show that the packing of AXXXA motifs strongly stabilizes the 1TM–2TM helix bundle, although it did not promote the formation of the 1TM–1TM bundle.

Membrane cholesterol further stabilized the 1TM–2TM bundle ($\Delta\Delta G_a$ = –9 kJ mol^{-1}, Table 2). A characteristic large tilt of the helix (30 ± 1°, Table 3) suggests the formation of a more tilted helix bundle with less optimal side-chain packing, compensating for a high lateral pressure at the

center of cholesterol-containing membranes, similar to the 1TM–1TM bundle (Figure 6) [23]. Interestingly, smaller enthalpy–entropy compensation was observed for the 1TM–2TM association (ΔH_a = –59 kJ mol^{-1}, $-T\Delta S_a$ = +31 kJ mol^{-1}, Table 2), compared with those for the 1TM–1TM (ΔH_a = –84 kJ mol^{-1}, $-T\Delta S_a$ = +61 kJ mol^{-1}) and 2TM–2TM associations (ΔH_a = –109 kJ mol^{-1}, $-T\Delta S_a$ = +84 kJ mol^{-1}), suggesting the presence of entropically favorable and enthalpically unfavorable factors that stabilize the 1TM–2TM bundle in the presence of cholesterol. The large tilt angle suggests the existence of multiple/flexible structures, which can increase entropy and enthalpy of the dimer state. This is also consistent with the observed shorter monomer lifetime for the 1TM–2TM association in the presence of cholesterol (Table 1, 159 ms). That is, the probability of dimer formation increases upon the collision of two monomers.

2TM–2TM bundle. Strong 2TM–2TM associations were observed in both POPC and POPC/cholesterol bilayers. The maximum helix macrodipole interaction in the 2TM–2TM bundle (Figure 7b) was calculated according to Eq. (1) assuming two attractive and two repulsive interactions at distances of 10 Å and 10 $\times\sqrt{2}$ Å, respectively. The estimated ΔH value (–29.6 kJ mol^{-1}) explained roughly half of the observed ΔH_a value in POPC (–54.7 kJ mol^{-1}, Table 2). Therefore, the helix packing should also significantly contribute to ΔH_a (~–25 kJ mol^{-1}). However, this contribution was mostly compensated for by an increase in the entropic term $-T\Delta S_a$ (+25 (= 33 – 8) kJ mol^{-1}), which was indirectly estimated assuming the motional contribution of the +8 kJ mol^{-1} to $-T\Delta S_a$ term. The helix tilt angle increased to ~22° for 2TM compared with ~0° for 1TM (Table 3), consistent with formation of the 2TM–2TM bundle with a distinct structure by helix packing. In summary, the formation of the 2TM–2TM bundle is driven by helix macrodipole attractions (~–30 kJ mol^{-1}), and it accompanies close helix packing, although the packing does not strongly contribute to ΔG_a due to an enthalpy–entropy compensation.

Membrane cholesterol only slightly affected the stability ($\Delta\Delta G_a$ = –3 kJ mol^{-1}, Table 2), and did not alter the helix tilt (22 ± 1° vs 23 ± 3°, Table 3) of the 2TM–2TM bundle, in contrast to the cases of 1TM–1TM and 1TM–2TM bundles. Monomeric 2TM helices could already tilt and form an hourglass-shaped helix-loop-helix structure to relieve the lateral pressure. The pentaglycine linker (~ 18 Å in extended structure) allows maximally ~35° tilt of the helices to form such helix-loop-helix structure. Overall, the observed weak cholesterol effect suggests that the contributions from helix–helix interactions become dominant for the 2TM–2TM associations.

5. CONCLUSION

This study revealed that both changes in the of number of membrane-spanning segments and involvement of membrane cholesterol could significantly alter the stabilities and structures of helix bundles in membranes. In previous studies, we found that basal properties of 1TM principally originated from the helix macrodipole. Consistently, we observed that the change in the pattern of helix dipole interactions markedly affected both thermodynamic and kinetic stabilities of the 1TM–1TM, 1TM–2TM, and 2TM–2TM bundles. Such a tendency should be general for TM helix bundles with naturally occurring sequences, although the helix-packing contributions are sequence-dependent. Furthermore, we found that cholesterol strongly induced the formation of bundles with tilted helices for smaller numbers of membrane-spanning segments (two or three), whereas it is not so influential in the presence of a larger number of membrane-spanning segments (four). Particularly, the combination of the 1TM–2TM bundle and cholesterol resulted in the formation of a unique helix bundle with large helix tilt and high thermodynamic stability. The above results suggest that folding units composed of small numbers of membrane-spanning segments can be highly susceptible to membrane cholesterol. Such a protein unit may be useful, for example, as a dynamic switch sensitive to membrane physico-chemical properties. The concentration of peptides would also affect the bilayer thickness and tilt of the peptides. This study was done at low peptide

concentrations and it would be interesting to study higher concentrations in future. Quantitative information on the basal interactions that stabilize transmembrane proteins obtained in this study is also critical to correctly evaluate specific interactions when guest amino acids are introduced into the sequence.

REFERENCES

[1] G.G. Gregorio, M. Masureel, D. Hilger, D.S. Terry, M. Juette, H. Zhao, Z. Zhou, J.M. Perez-Aguilar, M. Hauge, S. Mathiasen, J.A. Javitch, H. Weinstein, B.K. Kobilka, S.C. Blanchard, Single-molecule analysis of ligand efficacy in β2AR-G-protein activation, Nature, 547 (2017) 68–73.

[2] E.O. Grushevskyi, T. Kukaj, R. Schmauder, A. Bock, U. Zabel, T. Schwabe, K. Benndorf, M.J. Lohse, Stepwise activation of a class C GPCR begins with millisecond dimer rearrangement, Proc. Natl. Acad. Sci. U.S.A., 116 (2019) 10150–10155.

[3] Y. Kofuku, T. Ueda, J. Okude, Y. Shiraishi, K. Kondo, T. Mizumura, S. Suzuki, I. Shimada, Functional dynamics of deuterated β2-adrenergic receptor in lipid bilayers revealed by NMR spectroscopy, Angew. Chem. Int. Ed. Engl., 53 (2014) 13376–13379.

[4] M.J. Lohse, K.P. Hofmann, Spatial and Temporal Aspects of Signaling by G-Protein-Coupled Receptors, Mol. Pharmacol., 88 (2015) 572–578.

[5] J.A. Hern, A.H. Baig, G.I. Mashanov, B. Birdsall, J.E. Corrie, S. Lazareno, J.E. Molloy, N.J. Birdsall, Formation and dissociation of M1 muscarinic receptor dimers seen by total internal reflection fluorescence imaging of single molecules, Proc. Natl. Acad. Sci. U.S.A., 107 (2010) 2693–2698.

[6] R.E. Jefferson, T.M. Blois, J.U. Bowie, Membrane proteins can have high kinetic stability, J. Am. Chem. Soc., 135 (2013) 15183–15190.

[7] R.E. Jefferson, D. Min, K. Corin, J.Y. Wang, J.U. Bowie, Applications of Single-Molecule Methods to Membrane Protein Folding Studies, J. Mol. Biol., 430 (2018) 424–437.

[8] R.S. Kasai, A. Kusumi, Single-molecule imaging revealed dynamic GPCR dimerization, Curr. Opin. Cell Biol., 27 (2014) 78–86.

[9] R. Lamichhane, J.J. Liu, K.L. White, V. Katritch, R.C. Stevens, K. Wuthrich, D.P. Millar, Biased Signaling of the G-Protein-Coupled Receptor β2AR Is Governed by Conformational Exchange Kinetics, Structure, 28 (2020) 371–377.

[10] R. Maeda, T. Sato, K. Okamoto, M. Yanagawa, Y. Sako, Lipid-Protein Interplay in Dimerization of Juxtamembrane Domains of Epidermal Growth Factor Receptor, Biophys. J., 114 (2018) 893–903.

[11] F. Cornelius, Modulation of Na,K-ATPase and Na-ATPase activity by phospholipids and cholesterol. I. Steady-state kinetics, Biochemistry, 40 (2001) 8842–8851.

[12] A.G. Lee, How lipids affect the activities of integral membrane proteins, Biochim. Biophys. Acta, 1666 (2004) 62–87.

[13] M. Stangl, D. Schneider, Functional competition within a membrane: Lipid recognition vs. transmembrane helix oligomerization, Biochim. Biophys. Acta, 1848 (2015) 1886–1896.

[14] E. van den Brink-van der Laan, J.A. Killian, B. de Kruijff, Nonbilayer lipids affect peripheral and integral membrane proteins via changes in the lateral pressure profile, Biochim. Biophys. Acta, 1666 (2004) 275–288.

[15] V. Anbazhagan, D. Schneider, The membrane environment modulates self-association of the human GpA TM domain--implications for membrane protein folding and transmembrane signaling, Biochim. Biophys. Acta, 1798 (2010) 1899–1907.

[16] H. Hong, T.M. Blois, Z. Cao, J.U. Bowie, Method to measure strong protein–protein interactions in lipid bilayers using a steric trap, Proc. Natl. Acad. Sci. U.S.A., 107 (2010) 19802–19807.

[17] H. Hong, J.U. Bowie, Dramatic destabilization of transmembrane helix interactions by features of natural membrane environments, J. Am. Chem. Soc., 133 (2011) 11389–11398.

[18] S. Mall, R. Broadbridge, R.P. Sharma, J.M. East, A.G. Lee, Self-association of model transmembrane α-helices is modulated by lipid structure, Biochemistry, 40 (2001) 12379–12386.

[19] A. Nash, R. Notman, A.M. Dixon, De novo design of transmembrane helix–helix interactions and measurement of stability in a biological membrane, Biochim. Biophys. Acta, 1848 (2015) 1248–1257.

[20] Y. Song, E.J. Hustedt, S. Brandon, C.R. Sanders, Competition between homodimerization and cholesterol binding to the C99 domain of the amyloid precursor protein, Biochemistry, 52 (2013) 5051–5064.

[21] E. Sparr, W.L. Ash, P.V. Nazarov, D.T. Rijkers, M.A. Hemminga, D.P. Tieleman, J.A. Killian, Self-association of transmembrane α-helices in model membranes: importance of helix orientation and role of hydrophobic mismatch, J. Biol. Chem., 280 (2005) 39324–39331.

[22] M.G. Teese, D. Langosch, Role of GxxxG Motifs in Transmembrane Domain Interactions, Biochemistry, 54 (2015) 5125–5135.

[23] Y. Yano, K. Kondo, R. Kitani, A. Yamamoto, K. Matsuzaki, Cholesterol-induced lipophobic interaction between transmembrane helices using ensemble and single-molecule fluorescence resonance energy transfer, Biochemistry, 54 (2015) 1371–1379.

[24] Y. Yano, K. Matsuzaki, Measurement of thermodynamic parameters for hydrophobic mismatch 1: self-association of a transmembrane helix, Biochemistry, 45 (2006) 3370–3378.

[25] Y. Yano, A. Yamamoto, M. Ogura, K. Matsuzaki, Thermodynamics of insertion and self-association of a transmembrane helix: a lipophobic interaction by phosphatidylethanolamine, Biochemistry, 50 (2011) 6806–6814.

[26] W.P. Russ, D.M. Engelman, The GxxxG motif: a framework for transmembrane helix-helix association, J. Mol. Biol., 296 (2000) 911–919.

[27] R.F. Walters, W.F. DeGrado, Helix-packing motifs in membrane proteins, Proc. Natl. Acad. Sci. U.S.A., 103 (2006) 13658–13663.

[28] S.Q. Zhang, D.W. Kulp, C.A. Schramm, M. Mravic, I. Samish, W.F. DeGrado, The membrane- and soluble-protein helix-helix interactome: similar geometry via different interactions, Structure, 23 (2015) 527–541.

[29] K. Yamamoto, U.H. Durr, J. Xu, S.C. Im, L. Waskell, A. Ramamoorthy, Dynamic interaction between membrane-bound full-length cytochrome P450 and cytochrome b5 observed by solid-state NMR spectroscopy, Sci. Rep., 3 (2013) 2538.

[30] K. Yamamoto, M. Gildenberg, S. Ahuja, S.C. Im, P. Pearcy, L. Waskell, A. Ramamoorthy, Probing the transmembrane structure and topology of microsomal cytochrome-p450 by solid-state NMR on temperature-resistant bicelles, Sci. Rep., 3 (2013) 2556.

[31] Y. Yano, K. Kondo, Y. Watanabe, T.O. Zhang, J.J. Ho, S. Oishi, N. Fujii, M.T. Zanni, K. Matsuzaki, GXXXG-Mediated Parallel and Antiparallel Dimerization of Transmembrane Helices and Its Inhibition by Cholesterol: Single-Pair FRET and 2D IR Studies, Angew. Chem. Int. Ed. Engl., 56 (2017) 1756–1759.

[32] N. Castillo, L. Monticelli, J. Barnoud, D.P. Tieleman, Free energy of WALP23 dimer association in DMPC, DPPC, and DOPC bilayers, Chem. Phys. Lipids, 169 (2013) 95–105.

[33] M.N. Nishizawa, K., Sequence-nonspecific stabilization of transmembrane helical peptide dimer in lipid raft-like bilayers in atomistic simulations. I. Dimerization free energy and impact of lipid–peptide potential energy, Ann. Biomed. Res., 1 (2018) 105.

[34] A.B. Pawar, S.A. Deshpande, S.M. Gopal, T.A. Wassenaar, C.A. Athale, D. Sengupta, Thermodynamic and kinetic characterization of transmembrane helix association, Phys. Chem. Chem. Phys., 17 (2015) 1390–1398.

[35] G.R. Bartlett, Phosphorus assay in column chromatography, J. Biol. Chem., 234 (1959) 466–468.

[36] Y. Yano, T. Takemoto, S. Kobayashi, H. Yasui, H. Sakurai, W. Ohashi, M. Niwa, S. Futaki, Y. Sugiura, K. Matsuzaki, Topological stability and self-association of a completely hydrophobic model transmembrane helix in lipid bilayers, Biochemistry, 41 (2002) 3073–3080.

[37] C. Joo, T. Ha, Preparing sample chambers for single-molecule FRET, Cold Spring Harb. Protoc., 2012 (2012) 1104–1108.

[38] S.A. McKinney, C. Joo, T. Ha, Analysis of single-molecule FRET trajectories using hidden Markov modeling, Biophys. J., 91 (2006) 1941–1951.

[39] S. Ramadurai, A. Holt, V. Krasnikov, G. van den Bogaart, J.A. Killian, B. Poolman, Lateral diffusion of membrane proteins, J. Am. Chem. Soc., 131 (2009) 12650–12656.

[40] L.M. Smith, J.L. Rubenstein, J.W. Parce, H.M. McConnell, Lateral diffusion of M-13 coat protein in mixtures of phosphatidylcholine and cholesterol, Biochemistry, 19 (1980) 5907–5911.

[41] D.W. Tank, E.S. Wu, P.R. Meers, W.W. Webb, Lateral diffusion of gramicidin C in phospholipid multibilayers. Effects of cholesterol and high gramicidin concentration, Biophys. J., 40 (1982) 129–135.

[42] E.S. Wu, C.S. Yang, Lateral diffusion of cytochrome P-450 in phospholipid bilayers, Biochemistry, 23 (1984) 28–33.

[43] F.A. Nezil, M. Bloom, Combined influence of cholesterol and synthetic amphiphillic peptides upon bilayer thickness in model membranes, Biophys. J., 61 (1992) 1176–1183.

[44] H. Yang, S. Yang, J. Kong, A. Dong, S. Yu, Obtaining information about protein secondary structures in aqueous solution using Fourier transform IR spectroscopy, Nat. Protoc., 10 (2015) 382–396.

[45] Y.B. Yu, P.L. Privalov, R.S. Hodges, Contribution of translational and rotational motions to molecular association in aqueous solution, Biophys. J., 81 (2001) 1632–1642.

[46] H. Heerklotz, A. Tsamaloukas, Gradual change or phase transition: characterizing fluid lipid-cholesterol membranes on the basis of thermal volume changes, Biophys. J., 91 (2006) 600–607.

[47] R.F. Epand, A. Ramamoorthy, R.M. Epand, Membrane lipid composition and the interaction of pardaxin: the role of cholesterol, Protein Pept. Lett., 13 (2006) 1–5.

[48] A. Ramamoorthy, D.K. Lee, T. Narasimhaswamy, R.P. Nanga, Cholesterol reduces pardaxin's dynamics-a barrel-stave mechanism of membrane disruption investigated by solid-state NMR, Biochim. Biophys. Acta, 1798 (2010) 223–227.

[49] C.J. Morton, M.A. Sani, M.W. Parker, F. Separovic, Cholesterol-Dependent Cytolysins: Membrane and Protein Structural Requirements for Pore Formation, Chem. Rev., 119 (2019) 7721–7736.

[50] R.S. Cantor, Lipid composition and the lateral pressure profile in bilayers, Biophys. J., 76 (1999) 2625–2639.

[51] R.S. Cantor, Size distribution of barrel-stave aggregates of membrane peptides: influence of the bilayer lateral pressure profile, Biophys. J., 82 (2002) 2520–2525.

[52] X. Feng, P. Barth, A topological and conformational stability alphabet for multipass membrane proteins, Nat. Chem. Biol., 12 (2016) 167–173.

Table 1. Average lifetimes of monomers and dimers at 298 K

	POPC		POPC/cholesterol (7/3)	
peptides	monomer lifetime (ms)	dimer lifetime (ms)	monomer lifetime (ms)	dimer lifetime (ms)
1TM–1TM	not detected	not detected	562	261
1TM–2TM	545	99	159	381
2TM–2TM	1000	394	567	478

Table 2. Thermodynamic parameters of the association of helices in POPC membranes at 298 K

Peptides	ΔG_a (kJ mol^{-1})			ΔH_a (kJ mol^{-1})			$-T\Delta S_a$ (kJ mol^{-1})		
	POPC	+chol	difference	POPC	+chol	difference	POPC	+chol	difference
1TM–1TM	–13.2 ± 0.2*	–22.6 ± 0.1**	–9.4	–23.7 ± 0.4*	–84.1 ± 1.7**	–60.4	+10.4 ± 0.4*	+61.4 ± 1.7**	+51.0
1TM–2TM	–19.3 ± 1.2	–28.3 ± 2.6	–9.0	–35.4 ± 1.0	–59.3 ± 3.2	–23.9	+16.1 ± 1.0	+31.0 ± 3.2	+14.9
2TM–2TM	–21.6 ± 2.2	–24.2 ± 3.1	–2.6	–54.7 ± 6.6	–109.1 ± 20	–54.4	+33.4 ± 6.6	+84.0 ± 20	+50.6

*data from ensemble measurements (assuming $\Delta C_{p(a)} = -0.5$ J K^{-1} mol^{-1})[25]

**data from ensemble measurements (assuming $\Delta C_{p(a)} = 1.5$ J K^{-1} mol^{-1})[23]

Table 3. FTIR–PATR parameters for assessment of helix orientation at 298 K

	POPC		POPC/cholesterol(7/3)	
Peptides	*R**	α* (deg)	*R*	α (deg)
1TM–1TM	6.5 ± 0.6	~0	4.7 ± 0.2	17 ± 2
1TM–2TM	4.8 ± 0.2	15 ± 3	3.6 ± 0.1	30 ± 1
2TM–2TM	4.3 ± 0.1	22 ± 1	4.2 ± 0.1	23 ± 3

* *R* and α indicate the dichroic ratio for the peptide amide I band and angle of helix orientation relative to the bilayer normal calculated from *R* (Eq. 1), respectively.

FIGURE LEGENDS

Figure 1. Single-pair FRET (sp-FRET) measurements. (a) Schematic illustration of a surface-attached vesicle for sp-FRET imaging by total internal reflection microscopy. (b) Representative time-courses of fluorescence intensities for Cy3B (green) and Cy5 (Red) under excitation of Cy3B for 1TM–1TM (left column), 1TM–2TM (middle column), and 2TM–2TM pairs (right column) in POPC (upper row) and POPC/cholesterol (lower row) at 25°C. The number of analyzed vesicles is denoted by *n*. Only Cy3B fluoresced for 1TM–1TM in POPC, indicating no association between the helices. Under other conditions, the emissions fluctuated with an anticorrelation, reflecting the association–dissociation dynamics of the helices. (c)(d) Photobleaching of Cy3B (c) and Cy5 (d) detected as a stepwise decrease in the fluorescence intensities (arrowheads). The vesicles that had incorporated one Cy3B-helix and one Cy5-helix were selected for analysis.

Figure 2. Sp-FRET analysis for 1TM–2TM and 2TM–2TM associations in POPC vesicles. (a) HaMMy fitting for sp-FRET trajectories assuming two-state transitions. Black and green lines indicate measured apparent FRET efficiency (E_{app}) and the most probable fitting, respectively. The monomer and dimer states correspond to E_{app} values of ~0.4 and ~0.8, respectively. (b) Histograms of natural logarithm of rate constants for dimer formation (k_{on}) and dimer dissociation (k_{off}). The average $\pm$ error values were obtained from Gaussian fitting of the histogram. (c) Histograms of E_{app}.

Figure 3. Sp-FRET analysis for 1TM–1TM, 1TM–2TM, and 2TM–2TM associations in POPC/cholesterol (7/3) vesicles. (a) Histograms of the natural logarithm of rate constants for dimer formation (k_{on}) and dimer dissociation (k_{off}). The average $\pm$ error values were obtained from Gaussian fitting of the histogram. (b) Histograms of E_{app}.

Figure 4. Temperature dependences of association free energy for (a) 1TM–2TM associations and (b) 2TM–2TM associations. The temperature dependences were linearly fitted to estimate the thermodynamic parameters by Eq. (7).

Figure 5. Amide region FTIR-PATR spectra for 1TM, 1TM/2TM(1/1) or 2TM incorporated into membranes (peptides/lipids = 1/1000) at 25°C. The membrane films were hydrated with D_2O vapor. Red and black lines indicate raw spectra for the IR beam with its electric vector parallel and perpendicular to the plane of incidence, respectively.

Figure 6. Effects of the membrane lateral pressure profile on the shape of the transmembrane helix bundle. Because of the small headgroup of cholesterol, the headgroup and hydrocarbon core regions have lower and higher lateral pressures, respectively, in cholesterol-containing membranes (red arrows), compared with in pure POPC membranes. POPC membranes stabilize helix bundles without helix tilt (parallel helix bundle). On the other hand, cholesterol-containing membranes can stabilize helix bundles with significant helix tilt (hourglass-shaped helix bundle).

Figure 7. Alterations in the helix macrodipole interactions upon the formation of the 1TM–2TM bundle (a) and 2TM–2TM bundle (b). Upward and downward arrows in the circles indicate C-terminus-up and C-terminus-down transmembrane topologies of the helices, respectively. Antiparallel (A) and parallel (P or P') interhelical contacts are shown as blue and red lines, respectively. (a) 1TM–2TM association generates A + P interactions, which is zero assuming symmetric packing of the helices in the bundle. (b) The repulsive interactions in 2TM–2TM bundle are minimized in square packing (P'). The association generates 2A + 2P' interactions, which have a negative ΔH value.

Figure 1

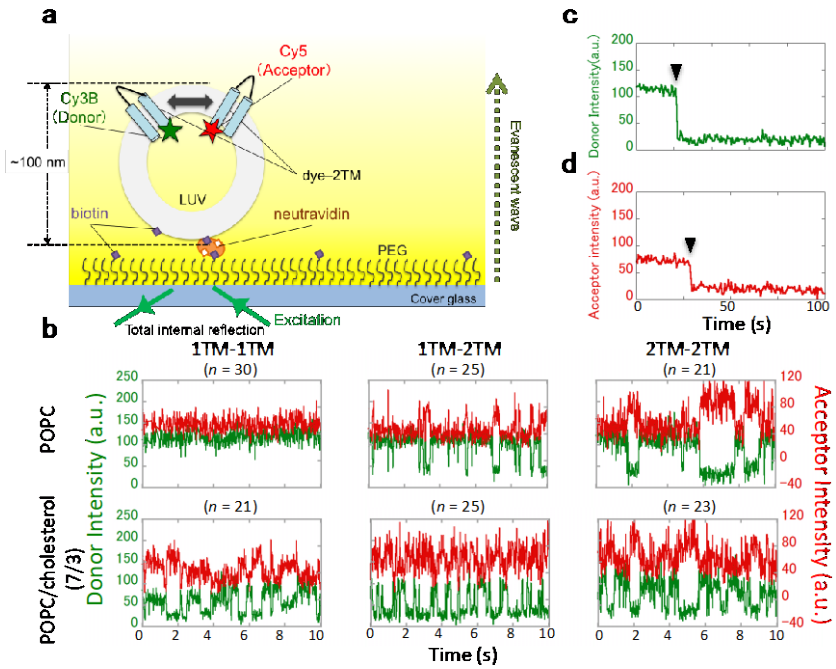
a
Cy5
(Acceptor)
Cy3B
(Donor)
~100 nm
dye–2TM
LUV
biotin
neutravidin
PEG
Cover glass
Evanescent wave
Total internal reflection
Excitation
c
Donor Intensity(a.u.)
d
Acceptor intensity (a.u.)
Time (s)
b
1TM-1TM
1TM-2TM
2TM-2TM
(n = 30)
(n = 25)
(n = 21)
(n = 21)
(n = 25)
(n = 23)
POPC
POPC/cholesterol (7/3)
Donor Intensity (a.u.)
Acceptor Intensity (a.u.)
Time (s)

Figure 2

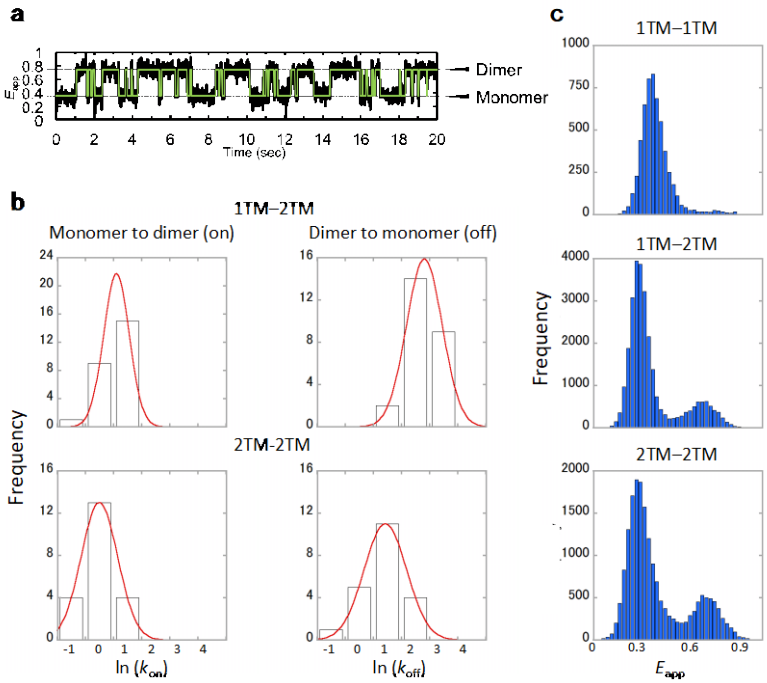
a
Dimer
Monomer
Time (sec)
b
1TM–2TM
Monomer to dimer (on)
Dimer to monomer (off)
2TM-2TM
Frequency
ln (k_{on})
ln (k_{off})
c
1TM–1TM
1TM–2TM
2TM–2TM
Frequency
E_{app}

Figure 3

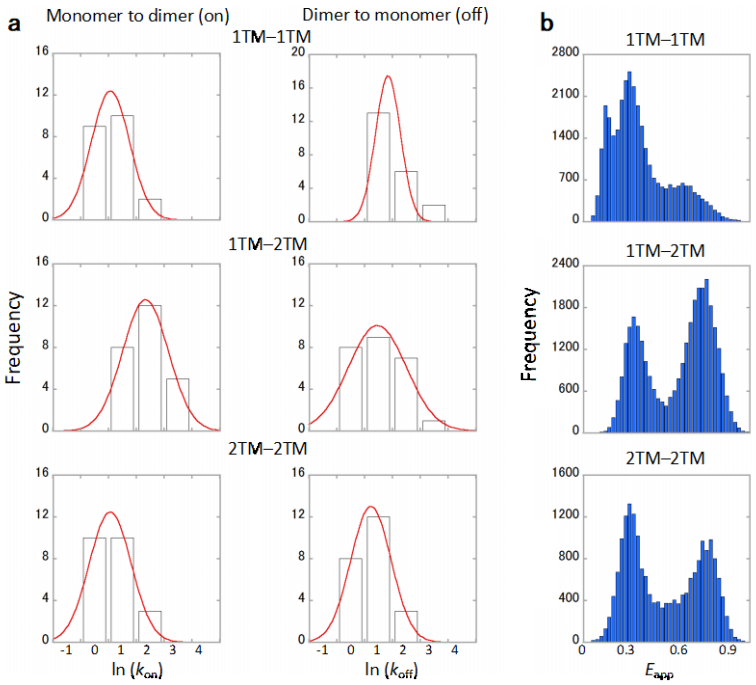
a
Monomer to dimer (on)
Dimer to monomer (off)
1TM–1TM
1TM–2TM
2TM–2TM
Frequency
ln (k_{on})
ln (k_{off})
b
1TM–1TM
1TM–2TM
2TM–2TM
Frequency
E_{app}

Figure 4

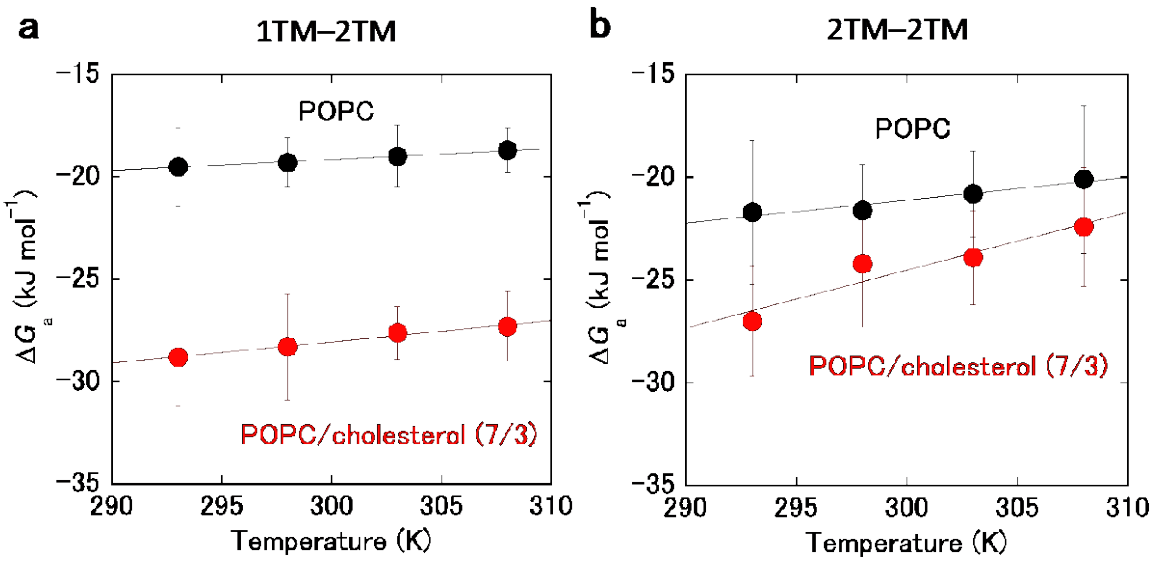
a
1TM–2TM
POPC
POPC/cholesterol (7/3)
ΔG a (kJ mol−1)
Temperature (K)
b
2TM–2TM
POPC
POPC/cholesterol (7/3)
ΔG a (kJ mol−1)
Temperature (K)

Figure 5

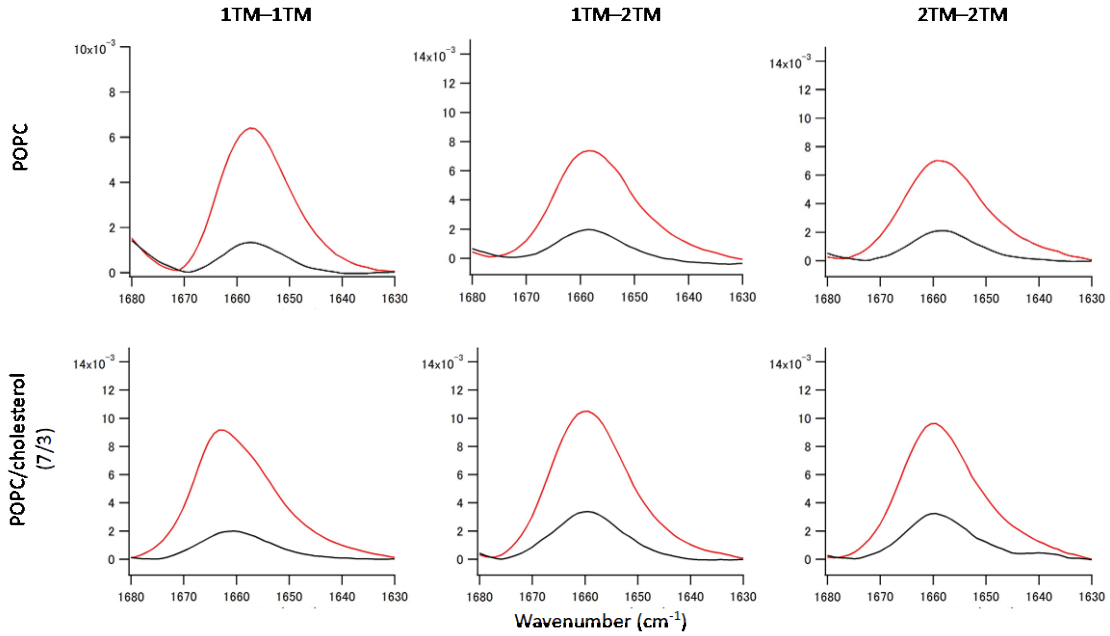
1TM–1TM
1TM–2TM
2TM–2TM
POPC
POPC/cholesterol (7/3)
Wavenumber (cm-1)

Figure 6

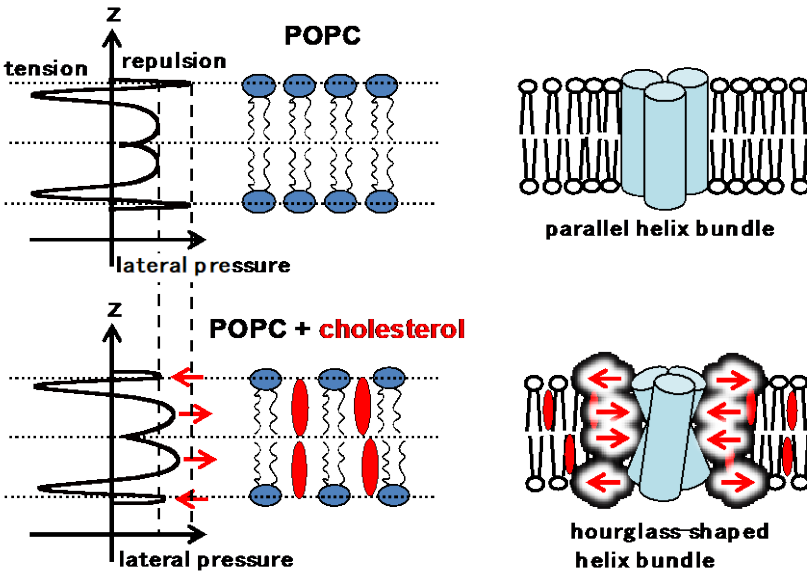
z
POPC
tension
repulsion
lateral pressure
parallel helix bundle
z
POPC + cholesterol
lateral pressure
hourglass-shaped
helix bundle

Figure 7

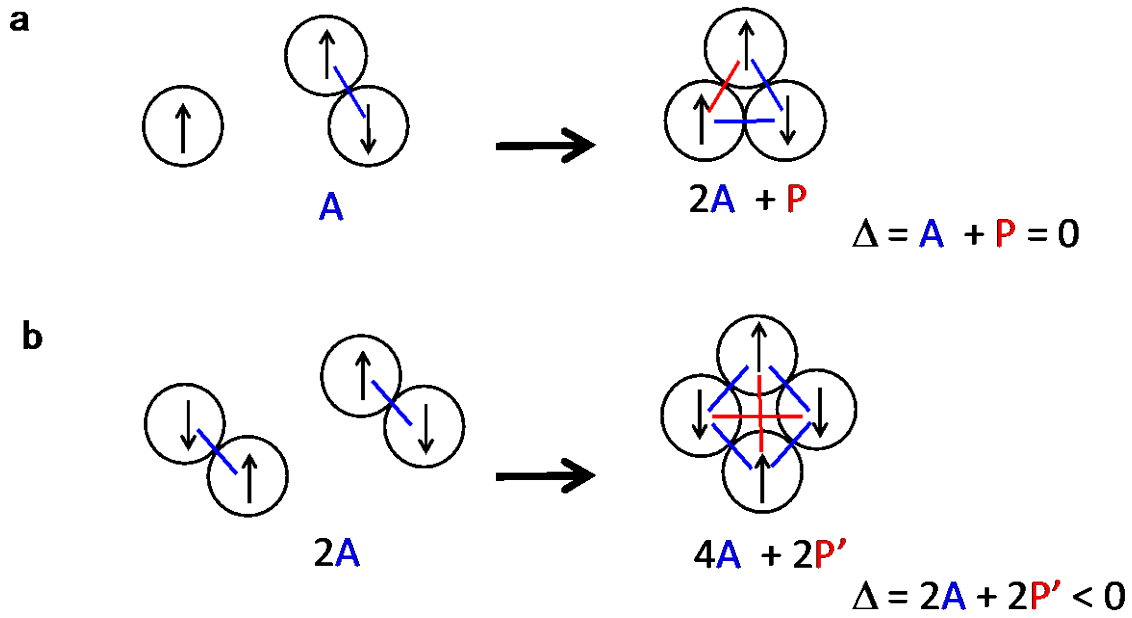

Supporting information

Thermodynamic and kinetic stabilities of transmembrane helix bundles as revealed by single-pair FRET analysis: Effects of the number of membrane-spanning segments and cholesterol

Yoshiaki Yano, Yuta Watanabe, and Katsumi Matsuzaki

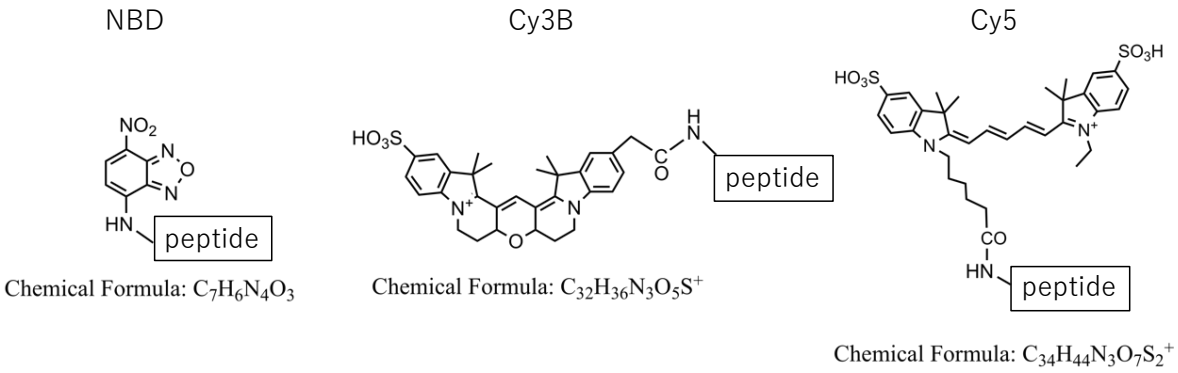

Figure S1. Structures of florescent probes used in this study.

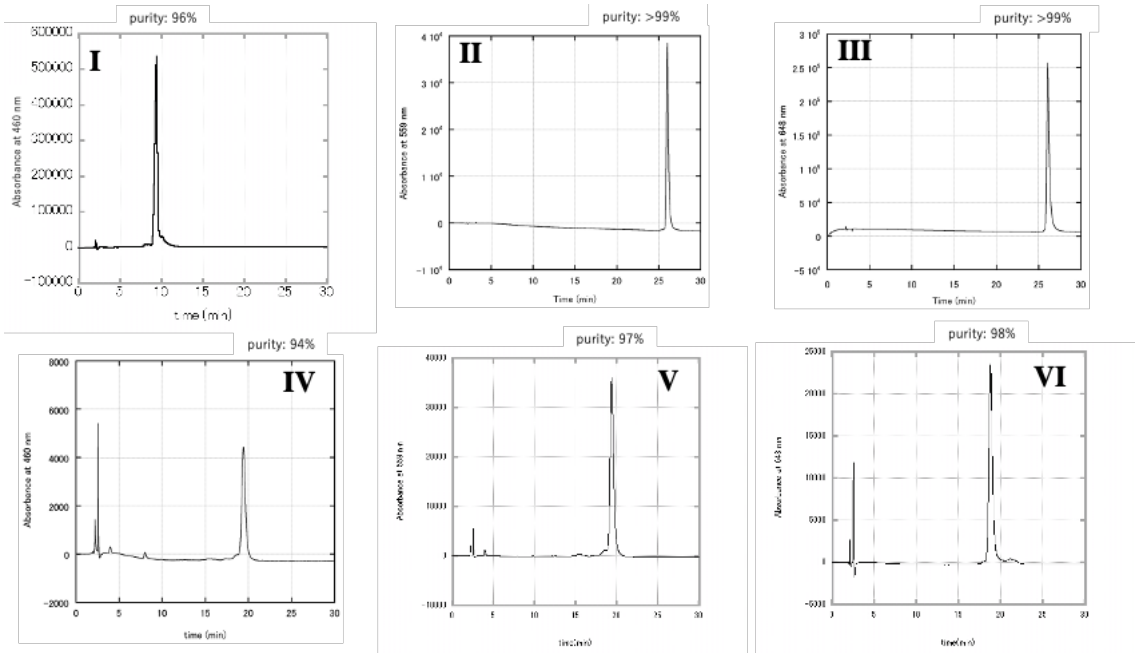

Figure S2. HPLC chromatograms of transmembrane peptides. Purified fluorophore-labeled peptides (**I**–**VI**) were analyzed with a PLRP-s analytical column (150×4.6 mm) at 50°C. The 1TM peptides were eluted with a linear gradient of H_2O/0.1% TFA and AcCN/0.1% TFA from 65 to 95% (**I**), and from 10 to 90% (**II**, **III**). The 2TM peptides (**IV**, **V**, **VI**) were eluted with a linear gradient of formic acid/H_2O (2/3, v/v) and formic acid/2-propanol (4/1, v/v) from 50 to 80% (0–5min) and 80 to 95% (5–30 min).